communications earth & environment

Article

A Nature Portfolio journal

https://doi.org/10.1038/s43247-025-02400-3

Land use and mineral type determine stability of newly formed mineral-associated organic matter

Check for updates

De Shorn E. Bramble[1,2] ✉, Ingo Schöning[1], Luise Brandt[3], Christian Poll[3], Ellen Kandeler[3], Susanne Ulrich[4], Robert Mikutta[4], Christian Mikutta[5], Whendee L. Silver[6], Kai Uwe Totsche[2], Klaus Kaiser[4] & Marion Schrumpf[1] ✉

Formation of mineral-associated organic matter (MAOM) is a key process in the global carbon cycle, stabilising organic carbon in soils. The relative importance of mineral composition and land use as potential controls of MAOM stability at regional scales and underlying microbial processes are still unresolved. Here, we assessed the stability of MAOM formed on goethite (iron oxide) and illite (phyllosilicate clay) exposed for five years in topsoils at 68 forest and grassland sites across Germany. We incubated the newly formed MAOM, determined its extractability, and analysed the composition and functioning of associated microbial communities. Decomposition of MAOM was always significantly lower for goethite than illite, highlighting that higher organic carbon accumulation on goethite was not exclusively due to its larger sorption capacity. Instead, reduced organic carbon extractability and higher phosphorus-acquiring enzyme activities indicated stronger substrate limitation of microbial growth on goethite than illite. Across the two minerals, MAOM decomposition was consistently lower for forests than grasslands, relating to greater nutrient constraints and a different microbial community composition in forests. Overall, mineral type and land use explained 34.6 and 23.2% of the variance in MAOM decomposition. The pronounced land use effect on MAOM stability underlines its potential responsiveness to environmental change.

Our ability to optimise soil carbon (C) sequestration for climate change mitigation depends firmly on understanding the factors controlling the formation and stabilisation of organic matter (OM) in soils. Especially crucial to this effort is understanding the dynamics of mineral-associated OM (MAOM)—the OM fraction that accounts for more than 50% of soil organic C (OC)[1,2].

Mineral-associated OM in soil is presumed to consist of relatively low molecular weight organic compounds attached to mineral surfaces[3,4]. It is defined either as the OM in soil particle fractions smaller than 20–63 µm or having densities above 1.60–1.85 g cm^{-3} [4]. Minerals facilitate OM accumulation in soils by serving as sorbents for organic compounds and contribute to OM stabilisation by limiting its access to microorganisms and their enzymes, thereby protecting it from microbial decomposition and mineralisation[5–8]. Soil minerals, however, differ widely in their properties, and in turn, ability to accumulate and stabilise OM[5,8–12]. Hence, it is increasingly being recognised that soil OM storage and stabilisation depend firmly on the type and reactivity of minerals[11,13–16]. Due to their high abundance and reactivity, iron (oxyhydr)oxides (hereafter termed 'iron oxides') and phyllosilicate clays are considered the essential mineral constituents controlling the accumulation and stabilisation of OM in soils. Yet, these mineral groups will affect these soil processes differentially[5,12,16]. Iron oxides are predominately positively charged under acidic and circumneutral pH conditions, and thus sorb more OM than phyllosilicate clays. Phyllosilicate clays, in contrast, are predominately negatively charged and naturally repel negatively charged OM[8,12,17], given only minor amounts of divalent or trivalent cations are present in solution[17,18]. Binding of OM to iron oxides also mainly occurs via strong inner-sphere complexation (i.e., 'ligand exchange'), while binding to phyllosilicate clays is predominantly via

[1]Max Planck Institute for Biogeochemistry, Jena, Germany. [2]Department of Hydrogeology, Institute for Geosciences, Friedrich Schiller University Jena, Jena, Germany. [3]Department of Soil Biology, Institute of Soil Science and Land Evaluation, University of Hohenheim, Stuttgart, Germany. [4]Soil Science and Soil Protection, Martin Luther University Halle-Wittenberg, Halle (Saale), Germany. [5]Soil Mineralogy, Institute of Earth System Sciences, Gottfried Wilhelm Leibniz University Hannover, Hannover, Germany. [6]Department of Environmental Science, Policy, and Management, University of California Berkeley, Berkeley, CA, USA. ✉e-mail: dbramble@bgc-jena.mpg.de; mschrumpf@bgc-jena.mpg.de

presumably weaker cation bridging[5,8]. Therefore, OM associated with iron oxides is assumed to be less desorbable and, thus, overall more stable than OM associated with phyllosilicate clays. Empirical evidence to support this notion is, however, mainly derived from MAOM prepared in the laboratory under conditions that hardly reflect the wide range of environmental conditions in natural soils[5,9,10,19–21]. For instance, the organic compounds used to prepare MAOM in laboratory studies do not represent the full range of chemical and biological complexity and diversity of organic inputs under field conditions. Since organic compounds interact with iron oxides and phyllosilicate clays differently[10,12,22], with consequences for the stability of sorbed OM[5,9,10,20], it needs to be clarified whether and to what extent laboratory results are transferable to field conditions where the composition of the organic compounds contributing to MAOM formation is likely to be spatially and temporally heterogeneous.

Previous laboratory studies have also mainly focused on the abiotic factors affecting the differential stability of iron oxide versus phyllosilicate clay-associated OM, and comparably little attention has been given to the biological drivers involved (but see Konrad et al.[10]). It is important to advance our mechanistic understanding of the interplay of mineral type and mineral-associated microbial communities in MAOM cycling, as this knowledge can inform microbially explicit models for improved prediction of the response of soil OC to global change. In a previous field study with minerals exposed for five years to varying natural soil conditions, including different land use types and land management intensities, as well as geologic and pedogenic settings, we observed consistently higher microbial biomass per unit MAOM-C on illite (phyllosilicate clay) than on goethite (iron oxide)[23,24]. This suggests there was likely a lower bioavailability of OM and nutrients on goethite. We assumed that the higher microbial biomass on illite than goethite would be linked to faster cycling of OM associated with illite; however, this idea has not yet been tested.

In addition to mineral type, land use may shape soil microbial communities by modifying the amount and quality of organic inputs and soil conditions[25,26]. For instance, organic inputs in forests are often of lower quality (i.e., with a lower C:nutrient ratio and higher lignin content) than those in grasslands[27,28]. This imposes greater nutrient constraints on microbial activity in forests, causing slower decomposition of soil OM in that ecosystem compared to grasslands[29,30]. Moreover, the presence of higher-quality substrate may favour the proliferation of gram-negative

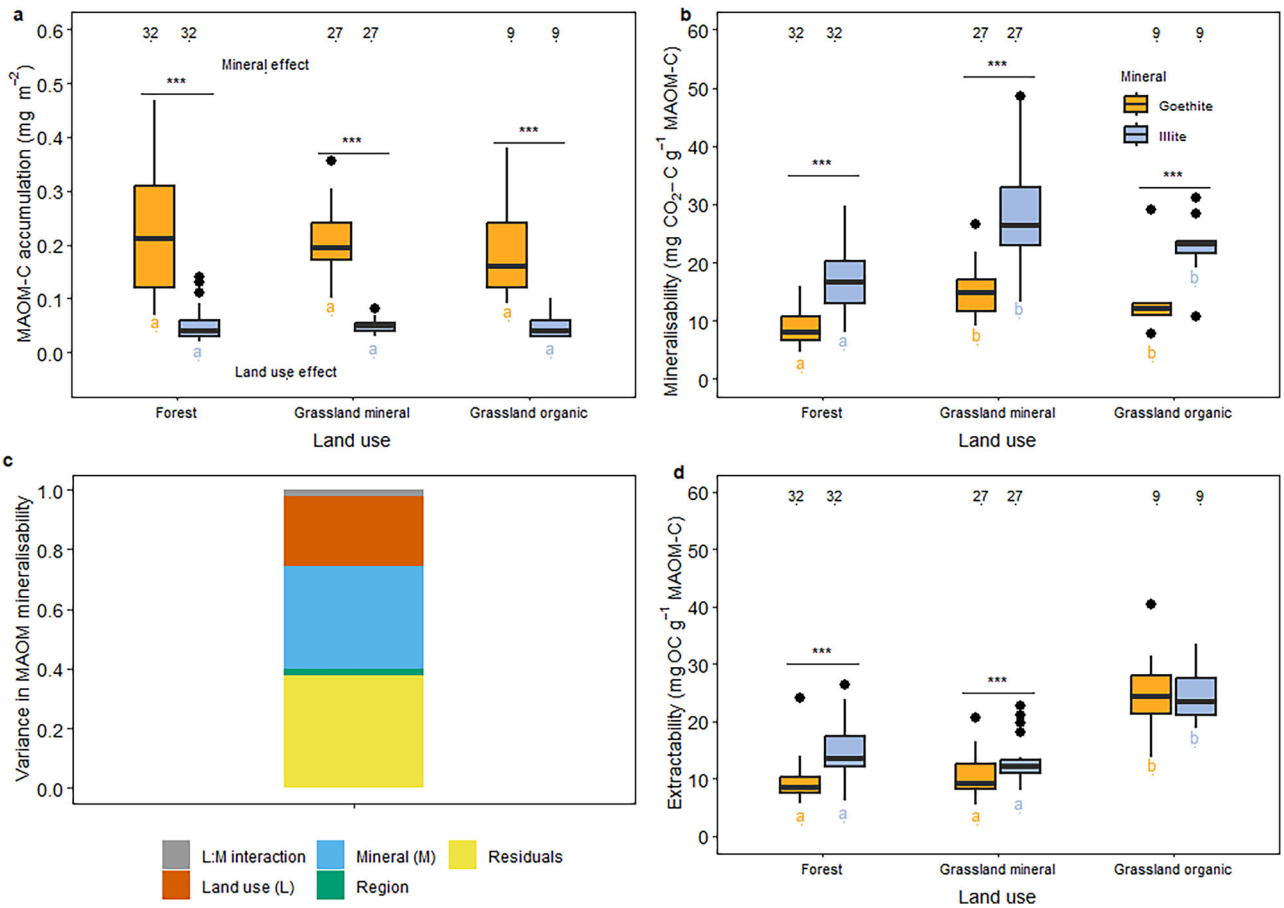

Fig. 1 | Amount and stability of mineral-associated organic matter (MAOM) accumulating on pristine minerals (goethite and illite) buried for five years at 5 cm depth in topsoils of forests and grasslands in three regions across Germany. a MAOM accumulation **b** MAOM mineralisability, **c** relative importance of study region, land use, mineral type, and the interactive effect of land use and mineral type (i.e., L:M interaction) on MAOM mineralisability, **d** MAOM extractability. The number of replicates of independent samples is given at the top of each box plot. The horizontal line within the box plot represents the median. The ends of the boxes represent the first and third quartiles, and the whiskers show the interquartile range (IQR) from the first and third quartiles. Black dots outside the whisker (i.e., 1.5 × IQR) of the plot represent outliers. Statistical significance for the individual and interactive effect of land use and mineral type was tested using analysis of variance (ANOVA). Study region was considered as a 'blocking' factor in the ANOVA. P-values, F-values, and effect sizes are presented in Supplementary Table S2. Statistical significance between means was determined using Tukey's honest significant difference test. *** denotes a significant ($P \leq 0.001$) difference between the two minerals with a given land use treatment. Within the same mineral type, different lowercase letters indicate a significant difference between land use treatments. Differences were significant at least at $P < 0.05$, except for the difference between mineralisability of goethite-forest and goethite-grassland organic treatments, which was significant at $P < 0.1$. Grassland mineral (grasslands on mineral soils); Grassland organic (grasslands on organic soils). Organic C concentration is expressed as mg C per m^2 mineral surface area. These values were corrected for initial (pre-field exposure) C concentrations. See Table S3 in Supplement 3 for C concentrations expressed per g dry sample.

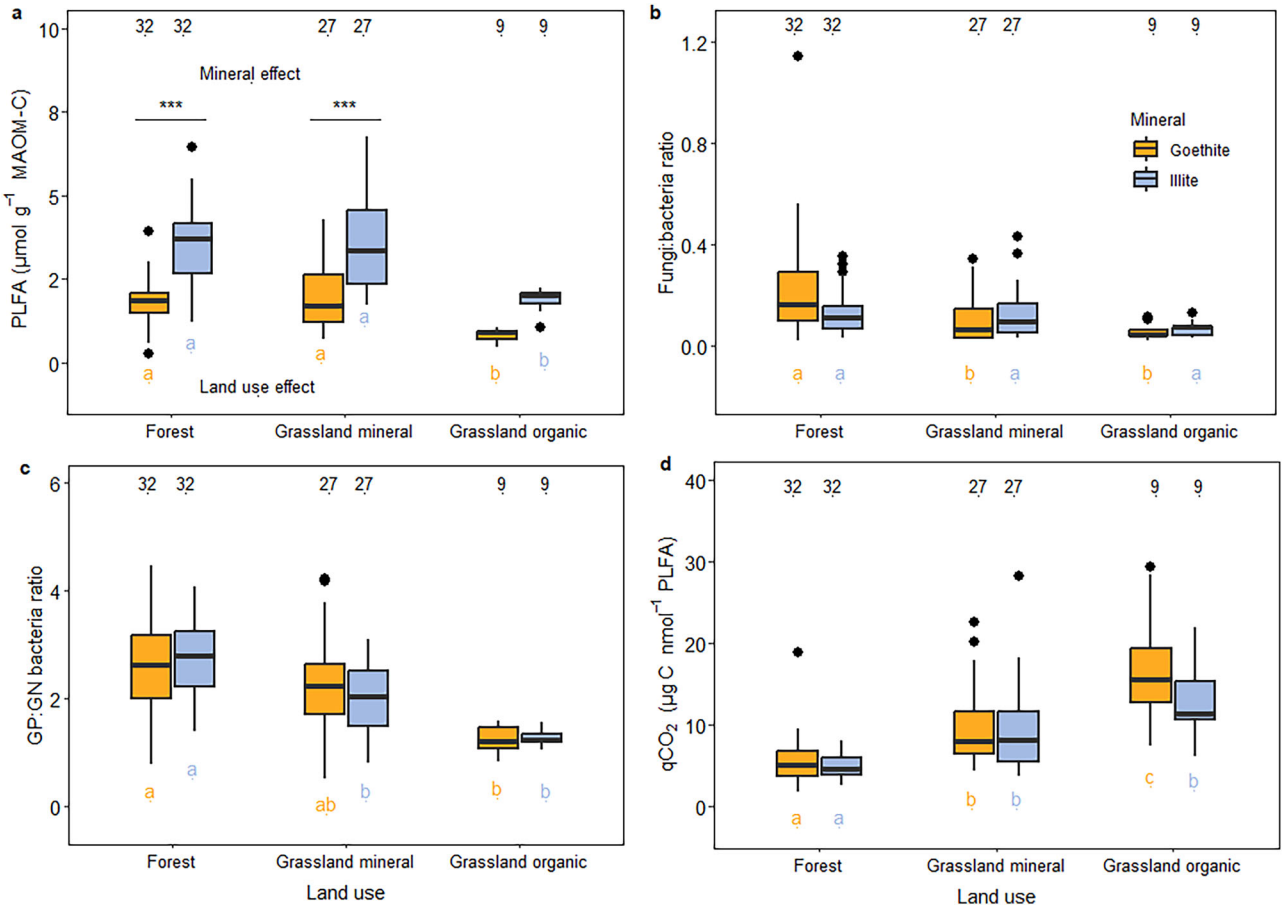

Fig. 2 | Effects of mineral type and land use on microbial properties of minerals (goethite and illite) buried for 5 years at 5 cm depth in forests and grasslands in three regions across Germany. a amount of phospholipid fatty acids (PLFA) per unit mineral-associated organic matter, **b** fungi:bacteria ratio, **c** gram-positive:gram-negative bacteria ratio, and **d** metabolic quotient of microbial communities. The number of replicates of independent samples is given at the top of each box plot. The horizontal line within the box plot represents the median. The ends of the boxes represent the first and third quartiles, and the whiskers show the interquartile range (IQR) from the first and third quartiles. Black dots outside the whisker (i.e., 1.5 × IQR) of the plot represent outliers. Statistical significance for the individual and interactive effect of land use and mineral type was tested using analysis of variance (ANOVA). Study region was considered as a 'blocking' factor in the ANOVA. P-values, F-values, and effect sizes are presented in Supplementary Table S2. Statistical significance between means was determined using Tukey's honest significant difference test. *** denotes a significant ($P \leq 0.001$) difference between the two minerals with a given land use treatment. Lowercase letters are used to indicate significant differences ($P < 0.05$) between land use treatments within the same mineral type lowercase. GP:GN bacteria ratio (gram-positive:gram-negative bacteria ratio); qCO_2 (PLFA-normalised CO_2 release; metabolic quotient); Grassland mineral (grasslands on mineral soils); Grassland organic (grasslands on organic soils.

bacteria[31,32], which, compared to most fungi and gram-positive bacteria, typically have low metabolic efficiency[33,34]. For this reason, a high abundance of gram-negative bacteria has been linked to faster decomposition of bulk OM[34]. However, whether this pattern translates to the MAOM fraction remains unknown.

In general, our understanding of the effects of land use-driven differences in organic input and microbial properties on MAOM decomposition is limited, partly owing to the dearth of studies on this topic and methodological challenges in measuring changes in the MAOM fraction of natural soils[12,35,36]. The presence of large amounts of MAOM from previous land uses and slow turnover time of MAOM, coupled with the substantial heterogeneity of minerals in fine soil particle size fractions and their different effects on OM cycling, can make it difficult to detect land use-driven effects on this OM fraction on short-time scales[12,35]. This point is exemplified in a regional-scale study where radiocarbon (^{14}C) was used to estimate the turnover times of C in various soil OM fractions of temperate forests and grasslands[35]. There, land use (forest versus grassland) significantly influenced the turnover of OM in fast cycling fractions (i.e., light and occluded particulate OM) but did not affect MAOM turnover[35]. In the current study, we overcame the methodological challenges involved in studying land use-driven effects on MAOM decomposition by leveraging a large-scale field experiment in which pristine minerals were exposed to natural soil conditions in differently managed temperate forests and grasslands[12].

The primary goal of this study was to compare the stability of MAOM formed on representatives of iron oxides and phyllosilicate clays after exposure to a wide range of environmental conditions in the field. Further, we aimed to clarify if and how MAOM stability is related to its chemical and microbial properties as imprinted by land use (forest versus grassland) and mineral type. We hypothesised that iron oxide-associated OM would be more stable (less mineralisable) than phyllosilicate clay-associated OM since iron oxides are capable of stronger binding of organic C and nutrients, which inhibits microbial life on that mineral compared to phyllosilicate clays. We further hypothesised that MAOM from forests would be less mineralisable than that from grasslands, linking to a higher relative abundance of fungi and higher microbial nutrient constraints in forests. To test these hypotheses, we exposed permeable containers with mixtures of either goethite (α-FeOOH; iron oxide) or illite (phyllosilicate clay) and quartz-sand for five years in topsoils of 32 forests and 36 grasslands (27 on mineral soils and 9 on organic soils) across three pedo-geologically distinct regions in Germany. The organic soils are the most alkaline of all soils (pH 5.5–7.6), which also experience extended periods of waterlogging because of raised water tables. Their inclusion in the study, therefore, allowed us to study

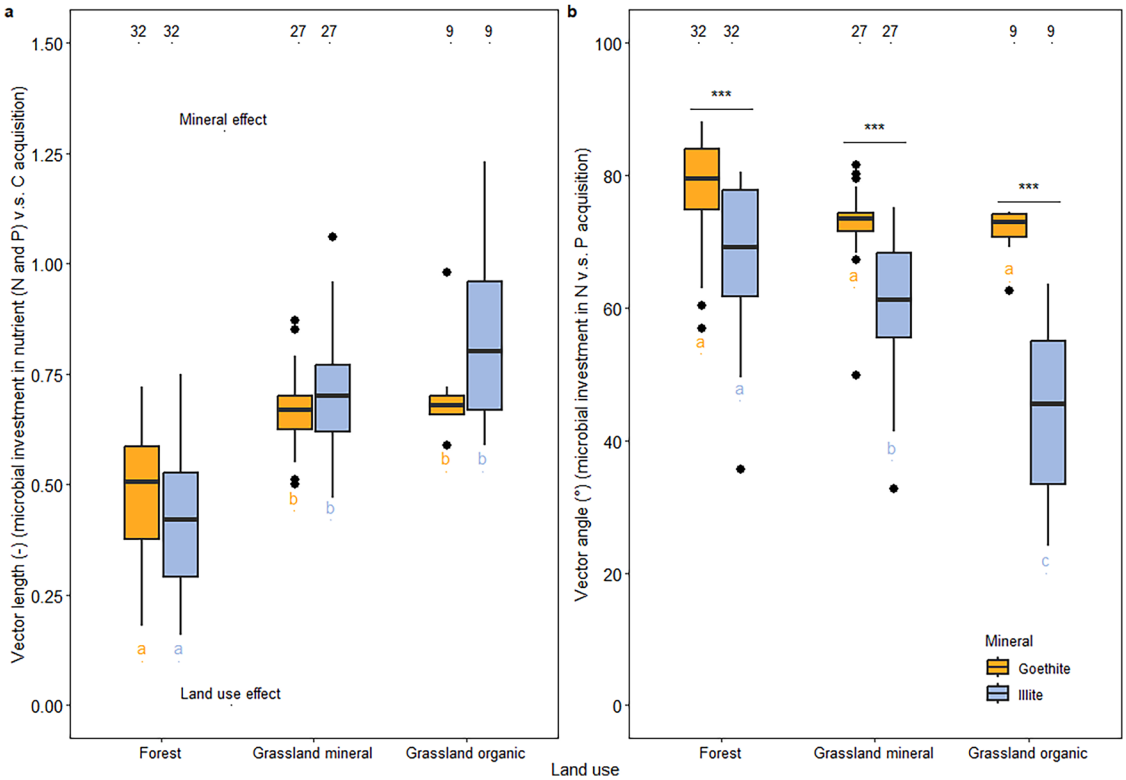

Fig. 3 | Effects of mineral type and land use on microbial investment in carbon and nutrient acquisition as revealed by enzymatic vector analysis. a vector lengths and **b** vector angles. Increasing vector length indicates an increase in microbial investment in carbon relative to nutrient (nitrogen and phosphorus) acquisition. Increasing vector angles indicate an increased microbial investment in phosphorus relative to nitrogen acquisition. The number of replicates (n) of independent samples is given at the top of each box plot. The horizontal line within the box plot represents the median. The ends of the boxes represent the first and third quartiles, and the whiskers show the interquartile range (IQR) from the first and third quartiles. Black dots outside the whisker (i.e., 1.5 × IQR) of the plot represent outliers. Statistical significance for the individual and interactive effect of land use and mineral type was tested using analysis of variance (ANOVA). Study region was considered as a 'blocking' factor in the ANOVA. P-values, F-values, and effect sizes are presented in Supplementary Table S2. Statistical significance between means was determined using Tukey's honest significant difference test. *** denotes a significant ($P \leq 0.001$) difference between the two minerals with a given land use treatment. Within the same mineral type, different lowercase letters indicate a significant difference between land use treatments. Differences were significant at least at $P < 0.05$, except for the difference between vector angles for illite-grassland mineral and illite-grassland organic which was significant at $P < 0.1$. Grassland mineral (grasslands on mineral soils); Grassland organic (grasslands on organic soils).

MAOM formation and stabilisation under field conditions considered less optimal for iron oxide-OM interactions (i.e., reduced conditions and pH >6.5)[14,37]. The mineral samples in the containers were separated from the surrounding soil with 50-µm mesh barriers, which prevented root ingrowth and mineral losses but allowed for water passage and microbial colonisation (Supplementary Fig. S1). We assessed the stability of MAOM as the mineralisability of OM associated with the field-exposed mineral samples by measuring the release of carbon dioxide (CO_2) per gram OC in laboratory incubations. To explore drivers of MAOM mineralisability we determined: (i) the proportion of MAOM-C extractable with $CaCl_2$ solution as an indicator of 'easily' extractable, more bioavailable, MAOM; (ii) the relative activities of extracellular enzymes involved in microbial acquisition of C, nitrogen (N), and phosphorus (P) to infer microbial limitation of C and nutrients; and (iii) the concentration of phospholipid fatty acids (PLFAs) on the mineral surfaces as an indicator of microbial biomass and composition. The approach of using the activity of extracellular enzymes to infer microbial limitation of C and nutrients is commonplace[38–41] and is based on the premise that microorganisms control enzyme production depending on their C and nutrient demands[39,42]. With our experimental setup and suite of chemical and microbial analyses, we sought to advance the contemporary understanding of the abiotic and microbial drivers of MAOM decomposition.

We show that decomposition of the newly formed MAOM is controlled both by land use and mineral type. We find lower MAOM decomposition for goethite than illite, which linked to a lower bioavailability of OC and P (i.e., lower extractable MOAM-C and greater P limitation), and smaller microbial biomass on goethite than illite. Irrespective of mineral type, MAOM decomposition was consistently lower for forests than grasslands, likely relating to stronger nutrient limitations and a lower abundance of gram-negative bacteria in forest. These findings indicate that MAOM decomposition is goverened not only by the amount of bioavailable C, but also by nutrient availability and physiological traits of associated microorganisms.

Results

Mineral-associated organic matter accumulation, mineralisability and extractability, as well as elemental ratios

After five years of field exposure, the amount of OC that accumulated per m^2 of mineral surface area was four times higher for goethite than illite (on average 0.21 ± 0.09 (standard deviation) and 0.05 ± 0.02 mg m^{-2} respectively; Fig. 1a). If OC concentration is expressed per gram of sample, it was three times higher for goethite than illite (Supplementary Table S1). The concentration of OC on the minerals did not differ between land uses (Fig. 1a; Supplementary Table S1).

Release of CO_2 per gram MAOM-C (i.e., MAOM mineralisability) during incubation of the field-exposed minerals under laboratory conditions ranged from 4.59 to 29 mg CO_2-C g^{-1} for goethite and 8.14 to 48.6 mg CO_2-C g^{-1} for illite (Fig. 1b; absolute CO_2 release data are presented in Supplementary Fig. S2). On average, MAOM mineralisability was two times higher for illite than goethite (Fig. 1b). The mineralisability of MAOM also

differed between land uses, being on average almost two times higher for grasslands than forests (Fig. 1b). We also observed a significant interaction between land use and mineral type on MAOM mineralisability (Supplementary Table S2), with the difference between forests and grasslands being greater for illite than goethite (Fig. 1b). Overall, mineral type emerged as the most important predictor in the linear model (ANOVA), explaining 34.6% of the variance in MAOM mineralisability. In comparison, land use explained 23.2% of the variance in MAOM mineralisability (Fig. 1c).

The extractability of MAOM (i.e., the proportion of newly formed MAOM-C extractable with 0.01 M $CaCl_2$) was higher for illite than goethite for the forest soils and grasslands on mineral soils (Fig. 1d), but did not differ between the two minerals in the grasslands on organic soils (24.4 ± 4.7 and 24.8 ± 8.1 mg OC g^{-1}) (Fig. 1d). Extractability of MAOM did not differ between grasslands and forests for minerals soils (Fig. 1d), while OM extractability was significantly higher for organic soils than mineral soils (Fig. 1d).

The C:N ratio of field-exposed goethite and illite samples was higher in forests than in grasslands (Supplementary Table S1). The ratios of C:P differed between the two minerals, being on average 3-fold higher for goethite than illite (Supplementary Table S1). Land use had a marginally significant effect on C:P ratios, with C:P ratios of forests being higher than grasslands (Supplementary Table S1).

Abundance, composition, and metabolic quotient of microbial communities

The concentration of PLFAs (an indicator for microbial biomass) expressed per gram of MAOM-C (PLFA:MAOM-C ratio) was significantly affected by mineral type (Supplementary Table S2), being on average two times higher on illite than goethite (Fig. 2a; absolute PLFA concentrations are presented in Supplementary Fig. S3). For both goethite and illite, the PLFA:MAOM-C ratio did not differ between forest and grasslands for mineral soils (Fig. 2a). The PLFA: MAOM-C ratio of the organic soils was significantly lower than mineral soils (Fig. 2a).

There was no effect of mineral type on the fungi:bacteria ratio, gram-positive:gram-negative bacteria ratio (GP:GN bacteria ratio), or the metabolic quotient (PLFA-normalised CO_2 release; qCO_2) of the microorganisms colonising the minerals' surfaces (Fig. 2b–d, Supplementary Table S2). These variables were significantly affected by land use (Supplementary Table S2). For goethite, both the fungi:bacteria ratio and GP:GN bacteria ratio were highest for forests and lowest for grassland-organic soils (Fig. 2b, c). The same trend was observed for illite, although differences between means were not always statistically significant (Fig. 2b, c). For both minerals, qCO_2 was about 2 to 3 times higher for grassland soils than forest soils (Fig. 2d).

Enzymatic carbon, nitrogen, and phosphorus acquisition

We measured the potential activities of enzymes involved in C (β-glucosidase, BG, and β-xylosidase, XYL), N (N-acetyl-β-glucosaminidase, NAG), and P (acid phosphatase, AP) acquisition (absolute and PLFA-normalised enzyme activities are presented in Supplementary Tables S3 and S4). Vector analysis was done on the ratios of these enzymes to infer microbial acquisition of C vs. N and P (vector length) and N vs. P (vector angle); see methods for details on this analysis. Vector lengths were similar between goethite (0.62) and illite (0.66). However, the effect of land use was significant (Supplementary Table S2). For both minerals, vector lengths were lower for forests than grasslands (Fig. 3a), suggesting lower investment in C relative to nutrient acquisition in forests. We also observed a significant interaction between land use and mineral type (Supplementary Table S2), where the difference between forest and grasslands was greater for illite than goethite (Fig. 3a).

In contrast to vector lengths, vector angles were significantly affected by mineral type (Supplementary Table S2), being higher for goethite than illite (Fig. 3b). Thus, compared to illite, microorganisms on goethite invested more in acquiring P than N. The interaction between land use and mineral type was also significant (Supplementary Table S2), with land use having a more substantial effect on vector angles for illite than goethite (Fig. 3b).

Table 1 | Linear mixed effect model and variance partitioning analysis exploring potential mechanisms underlying the land use effect on mineral-associated organic matter (MAOM) mineralisability

Parameter	Estimate	Std. Error	t value	*P* value	Variance Explained
Vector length	15.55	3.55	4.38	**<0.001**	0.070
#Fungi:bacteria	0.86	0.75	1.15	0.25	0.005
GP:GN bacteria	−2.05	0.70	−2.93	**0.003**	0.031
#BG:PLFA	−1.46	1.03	−1.41	0.16	0.008
#XYL:PLFA	0.36	0.56	0.67	0.51	0.002

Statistically significant effects ($P < 0.05$) are bold. R^2_m (correlation of determination for the effect of the fixed factors); R^2_c (correlation of determination for the effect of fixed and random factors). Vector length indicates microbial investment in C relative to nutrient (N and P) acquisition. Low vector lengths suggest possible nutrient limitation. GP:GN ratio (gram-positive:gram-negative bacteria ratio); PLFA (phospholipid fatty acids); BG: PLFA (PLFA-normalised β-glucosidase activity); XYL (PLFA-normalised β-xylosidase activity). $n = 136$. Marginal adjusted correlation of determination $R^2_m = 0.116$; $R^2_c = 0.594$; Mineral type and study region are considered random factors in the model; Root mean square error (RMSE) = 6.09; # Variables were log-transformed before running the model. Note: while the difference in soil pH between forests and grasslands might explain some of the variance in MAOM mineralisability, we did not include it in the presented model because we were mainly interested in the effects of microbial properties and nutrient availability on MAOM mineralisability. Noteworthy, however, is that the explained variance in MAOM mineralisability only increased by 1.4% when soil pH was considered in a separate model. This indicates that any non-microbial mediated effects of pH were likely small.

Mechanisms underlying mineral type and land use effects on MAOM mineralisability

We constructed linear mixed-effect models and performed variance partitioning analysis to investigate potential mechanisms that underlie the effects of land use and mineral type on MAOM mineralisability. For the 'land use effect model', we considered enzymatic vector lengths, fungi:bacteria ratio, GP:GN bacteria ratio, BG enzyme activity:PLFA ratio, and XYL enzyme activity:PLFA ratio as predictors of MAOM mineralisability (see statistical analyses for further details on variable selection). In this model, enzymatic vector lengths (indicator for nutrient limitation) and the ratio of GP:GN bacteria were the only statistically significant predictors of MAOM mineralisability. Both variables were positively related to MAOM mineralisability (Table 1). Most of the variability in MAOM mineralisability was explained by enzymatic vector lengths (indicator for nutrient limitation) in the 'land use effect' model (Table 1). The PLFA:MAOM-C, MAOM extractability, and enzymatic vector angles (indicator for P limitation) were considered as predictors in the 'mineral type effect' model. All variables in this model were significantly related to MAOM mineralisability. Specifically, MAOM mineralisability was positively related to PLFA:MAOM-C ratio and MAOM extractability, but negatively related to enzymatic vector angles (indicator for P limitation) (Table 2). The PLFA:MAOM-C ratio explained most of the variability in MAOM mineralisability in the 'mineral type effect' model (Table 2).

Discussion

Our study design allowed the disentangling of the influence of mineral type and land (i.e., difference in organic input quality and nutrients) on MAOM mineralisability. We found that more of the variance in MAOM mineralisability was explained by mineral type (34.6%) than by land use (23.2%), underlining the greater role of mineral type than land use in MAOM stabilisation. This finding has implications for modelling soil C dynamics since many of the existing soil C models (e.g., RothC and CENTURY) either underrepresent the role of mineral-organic associations in the stabilisation of soil OM or simply use clay content to modify the rate of OM decomposition and its transfer to slower cycling soil OM pools. Here, we provide direct evidence from a multi-year study to support the growing appeal to go beyond clay content—considering the type and reactivity of minerals—when modelling soil C dynamics[12,14,16,43,44]. Nonetheless, the fact that a considerable proportion of the variance in MAOM mineralisability was

Table 2 | Linear mixed effect model and variance partitioning analysis exploring potential mechanisms underlying the mineral type effect on mineral-associated organic matter (MAOM) mineralisability

Parameter	Estimate	Std. Error	t value	*P* value	Variance Explained
PLFA:MAOM-C	2.40	0.39	6.16	**<0.001**	0.173
[#]Extractability	4.91	1.51	3.24	**0.001**	0.069
[#]Vector angle	−12.93	2.52	−5.13	**<0.001**	0.116

Statistically significant effects ($P < 0.05$) are bold. PLFA: MAOM-C (phospholipid fatty acid concentration normalised to the content of MAOM). Vector angles indicate microbial investment in P relative to N acquisition. The higher the vector angles, the greater the investment in P acquisition. Higher vector angles allude to greater P limitation. R^2_m (correlation of determination for the effect of the fixed factors); R^2_c (correlation of determination for the effect of fixed and random factors). $n = 136$. Marginal adjusted correlation $R^2_m = 0.358$; Conditional adjusted correlation of determination $R^2_c = 0.638$; Land use and study region are considered as random factors in the model; Root mean square error (RMSE) = 5.31.
[#]Variables were log-transformed before running the model.

explained by land use is worth highlighting because it alludes to MAOM stability being an ecosystem feature. Indeed, this is an idea that is becoming increasingly popular in the scientific community[2,44–46].

For both goethite and illite, OM associated with minerals exposed at grassland sites was more mineralisable than those exposed at forest sites (Fig. 1a), supporting the hypothesis that MAOM from forests would be less decomposable (more stable) than that from grasslands. In contrast, the amount of MAOM formed did not differ between the two land use types (Fig. 1a). This is consistent with the findings of our previous study, where statistically significant differences between the two land use categories were only observed when forests were separated into coniferous and deciduous forests[12]. In that study, the amount of MAOM forming in topsoils was consistently higher under coniferous forests than in deciduous forests and grasslands, likely due to the thick surface organic layers in coniferous forests supplying large amounts of dissolved OM (DOM) to the mineral containers in the underlying topsoils[12]. By contrast, the overall difference between deciduous forests and grasslands was not statistically significant. Taken together, our results show that similar MAOM content between land uses does not necessarily imply the same stability.

Our study has certain limitations for extrapolating to natural soil systems, as it was conducted in an experimental setting. It is important to consider that the mineral containers were spatially separated from the surrounding soil, so that MAOM formation was likely driven mainly by percolation of DOM through the soil solution and microbial colonisation of the mineral surfaces. Furthermore, our laboratory-based assessment of MAOM stability does not account for the full range of processes in natural environments, such as rhizosphere interactions and redox dynamics. Nonetheless, we were able to elucidate how MAOM stability is influenced by its chemical and microbial characteristics, as shaped by land use and mineral type, thereby advancing the mechanistic understanding of these controlling factors.

Interestingly, land use patterns in MAOM mineralisability were consistent with the general trend in the mineralisability of OM in the bulk soil at our study sites[30] (Supplementary Table S5). This suggests that land use-driven effects on the decomposition of OM in the mineral fraction likely mirror those observed for the bulk soil. There are two likely explanations for the lower mineralisability of MAOM in forests than in grasslands in our study. Firstly, more significant nutrient limitation in forests than in grasslands, induced by the presence of lower quality OM (i.e., with higher C:nutrient ratios; Supplementary Table S1) in forests, might lead to slower OM decomposition in forests[27,35]. Indeed, we found that mineral-associated microorganisms invested more in nutrients than C acquisition in forests than grasslands (Fig. 3a), alluding to greater nutrient constraints in forests. Secondly, environmental conditions in grasslands (e.g., higher OM quality inputs, lower nutrient constraints, and higher soil pH) typically favour a greater abundance of gram-negative bacteria, with inherently lower metabolic efficiency[33,34,47], relative to fungi and gram-positive bacteria. Microbial communities with lower metabolic efficiency have been linked to faster cycling of soil OM[34,48]. Therefore, we surmise the higher relative abundance of gram-negative bacteria in grasslands than forests in our study (Fig. 2b, c) may have caused faster cycling of MAOM from grasslands. In support of this idea, we observed higher qCO_2 and activity (production) of C-acquiring enzymes per unit of microbial biomass in grasslands than in forests (Fig. 2d; Supplementary Table S4), which suggests a lower metabolic efficiency of mineral-associated microbial communities in grasslands[34,49].

Of the mechanisms likely underlying the land use effect on MOAM mineralisability, nutrient limitation (as indicated by enzymatic vector length) was the most important in our study (Table 1). However, we caution that the mechanisms underlying the land use effect are likely to be interdependent, and our study does not allow for full disentangling of their relative importance in the mineralisation of MAOM. This, therefore, remains a task for future studies.

Our study, which spanned a wide range of environmental conditions, provides direct and compelling evidence that OM in soils is more effectively stabilised by iron oxides than phyllosilicate clays. After five years of field exposure to the same environmental conditions, we found that irrespective of land use, much more OM accumulated on the tested iron oxide, goethite, than on the phyllosilicate clay, illite (Fig. 1a). Goethite-associated OM was also two times less mineralisable than illite-associated OM (Fig. 1b). Taken together, these results suggest a slower cycling of goethite- than illite-associated OM during the five-year time scale of our field experiment. This finding underscores that temperate soils rich in iron oxides likely have a higher capacity to store C for climate change mitigation than those dominated by phyllosilicate clays.

Interestingly, the difference in the mineralisability of goethite- and illite-associated OM was consistent with the direction and magnitude of difference in the ratio of PLFAs to MAOM-C on the minerals. Consequently, the difference in mineralisation between the two minerals was no longer significant when CO_2 release was normalised to their PLFA concentrations (Fig. 2d). This suggests that the greater release of CO_2 per unit MAOM-C of illite- than goethite-associated OM in our study was mainly caused by the higher abundance of microorganisms per unit MOAM-C on illite than goethite. It has been shown that the amount of CO_2 respired per unit microbial biomass (commonly referred to as the metabolic quotient, qCO_2) also depends on the microbial community composition[34,49]. Nevertheless, the composition of the microbial communities on the two minerals did not differ—at least by the used metrics—in our study (Fig. 2b, c). We also found that the PLFA:MOAM-C ratio was the most critical predictor of MAOM mineralisability among variables linked to the mineral type effect (Table 2). Our findings, thus, give insight into feedbacks between mineral type, the abundance of mineral-associated microorganisms, and the cycling of MAOM in soils. In doing so, our work advances the contemporary understanding of the role of microorganisms in the differential cycling of phyllosilicate clay- and iron oxide-associated OM in soils, going beyond previous studies at the laboratory scale that focused solely on the role of abiotic factors, such as OM binding strength[5,9].

The lower bioavailability of OM associated with iron oxides than phyllosilicate clays is often attributed to the surface properties of iron oxides that more strongly bind OM, which in turn reduces its potential to be desorbed[5,19,20]. Indeed, illite-associated OM was almost two times more extractable than goethite-associated OM for the forest soils and mineral soils of the grasslands (Fig. 1d). In contrast, in the organic soils of the grasslands, MAOM extractability was similar for illite and goethite (Fig. 1d), likely because goethite's OM stabilisation capability was significantly reduced due to the pH of these soils being close to the mineral's point of zero charge[12]. Despite this, goethite-associated OM from these soils was two times less mineralisable than illite-associated OM. Taken together, these results suggest that the extractability of MAOM alone—as estimated by extraction with $CaCl_2$—was not entirely indicative of MAOM bioavailability and usability. The fact that only 6.9% of the variance in MAOM mineralisability was explained by extractability in our study further strengthens this point

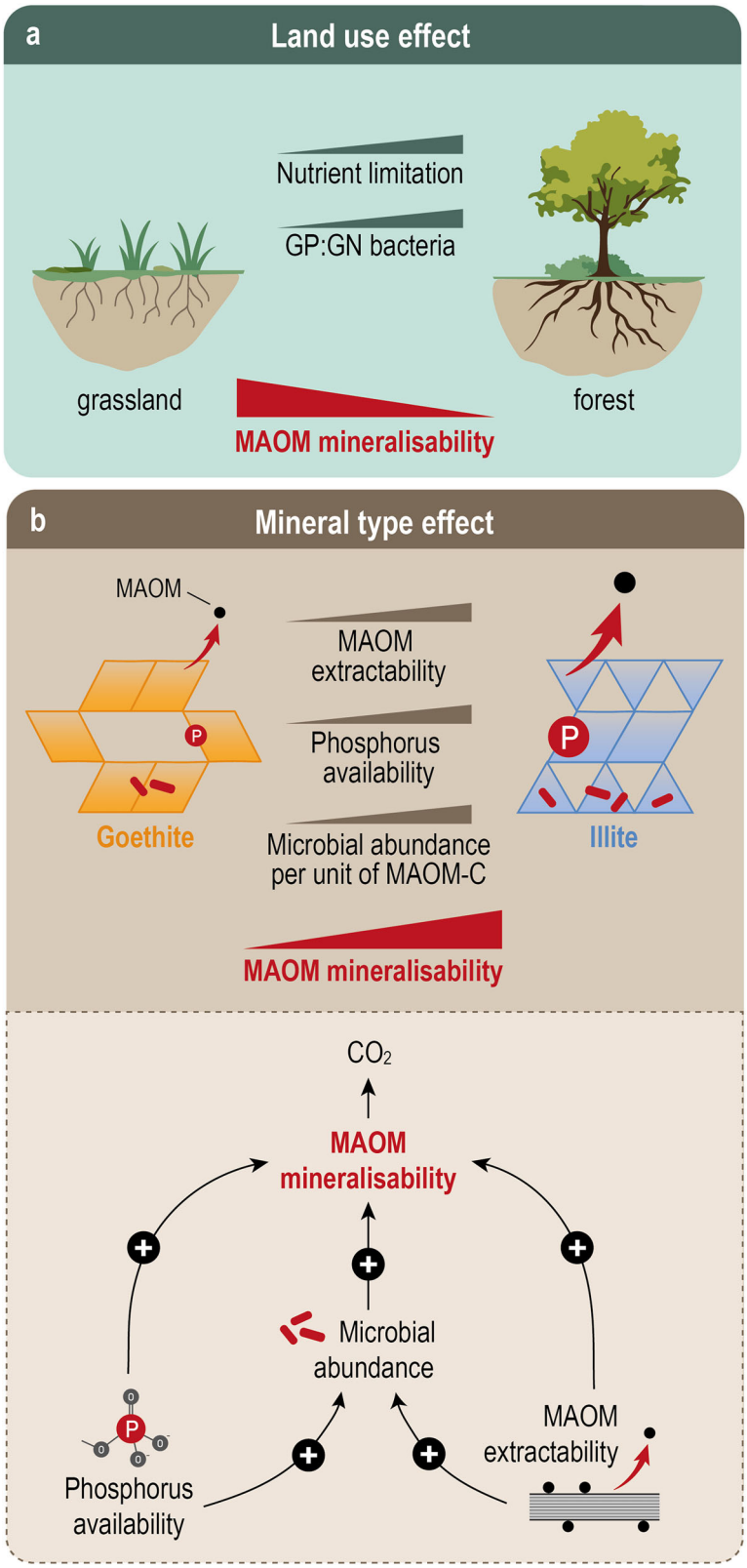

Fig. 4 | Graphical summary of the main findings of the study. a land use effect and **b** mineral type effect. GP:GN bacteria (gram-positive:gram-negative bacteria ratio). The bottom part of figure b illustrates a conceptual model of potential mechanisms underlying the differential mineralisability of goethite- and illite-associated organic matter (OM). The higher extractability of illite- than goethite-associated OM leads to greater accessibility of OM to illite-associated microbes, causing more significant loss of illite- than goethite-associated OM through microbial mineralisation. Higher extractability of illite-associated OM can cause higher microbial abundance on illite than goethite, leading to higher microbial mineralisation of illite- than goethite-associated OM. Alternatively, higher mineralisation of illite- than goethite-associated OM can be due to higher availability of phosphorus to illite- than goethite-associated microorganisms. Phosphorus availability may indirectly affect mineral-associated organic matter mineralisation through feedback on the abundance of mineral-associated microorganisms. The conceptual model is based on the results obtained in the current study. It does not preclude the importance of other parameters or mechanisms we did not assess.

(Table 2). Here, we suggest that greater nutrient constraints on goethite than illite might also partly explain the lower mineralisability of goethite-associated OM. We found similar enzymatic vector lengths (microbial investment in N and P relative to C acquisition) for both minerals, but significantly higher vector angles (microbial investment in N relative to P acquisition) for goethite than illite. This suggests that potential differences in the availability of nutrients on goethite and illite in our study might have been more strongly influenced by P than N. This finding aligns with the much greater difference (10–14 times) in the activity (production) of acid phosphatase (P cycling enzyme) than of N-acetyl-β-glucosaminidase (N cycling enzyme) per unit microbial biomass on the two minerals (Supplementary Table S4). Thus, higher vector angles—a variable that was negatively correlated with bioavailable organic P across different sites for both minerals[24]—for goethite than illite suggests microorganisms on goethite

were more limited by P than those on illite. The proposed lower availability of P on goethite than illite is consistent with the well-known fact that iron oxides bind phosphate stronger than phyllosilicate clays[17,22,50,51]. Variance partitioning analysis further revealed that more of the variability in MAOM mineralisability was explained by enzymatic vector angles (indicator for P limitation) than MAOM extractability (Table 2). This result suggests that decomposition of MAOM depended not only on the quantity of OM available to mineral-associated microorganisms but also on the presence of available nutrients. Moreover, it supports the idea that strong phosphate binding by goethite, leading to greater P limitation on goethite than illite, may have caused slower cycling of goethite-associated OM in our study. Our findings thus shed light on additional, and likely essential, mechanisms underlying the differential stability of phyllosilicate clay- and iron oxide-associated OM (Table 2; Fig. 4).

We observed a significant interaction between land use and mineral type where the difference in MAOM mineralisability between forests and grasslands was up to two times greater for illite than goethite (Fig. 1a). We suggest that this interaction might be partly explained by land use having a more substantial effect on nutrient constraints on illite than goethite (Fig. 3), where nutrients are likely anyways limited because of strong binding. Further research is, however, needed to validate this claim. Nonetheless, our findings suggest that OM in soils dominated by illite (and similar phyllosilicate clays) is likely to be more prone to losses upon environmental changes than OM in soils rich in goethite (and similar iron oxides). Our findings are likely most applicable to soils where oxic conditions prevail and the effect of oscillating redox reactions on the biogeochemical cycling of C and nutrients is minor, as these conditions closely match our laboratory incubations.

Conclusions

Our study illustrated the joint role of mineral type and land use-driven differences in soluble inputs and microbial properties in the decomposition of newly formed MAOM. The strong impact of land use on MAOM decomposition emphasises that MAOM is not an inert soil OM fraction but one that could be responsive to changing environmental conditions, even in the short term. Decomposition of MAOM from grasslands was faster than that from forests, likely in part due to less significant nutrient constraints on microbial activity and a higher abundance of gram-negative bacteria in grasslands. While further work is required to fully validate our findings, they raise the possibility of modifying land management practices to promote formation of persistent MAOM.

We found that irrespective of land use, goethite accumulated much more OM than illite. Goethite-associated OM was also less mineralisable than illite-associated OM. These findings suggest a slower cycling of goethite- than illite-associated OM in our experiment. Our work, therefore, underlines the superior OM accumulation and stabilising capability of iron oxides versus phyllosilicate clays across a broad range of environmental conditions on a multi-year time scale. It demonstrates that the very strong involvement of iron oxides in C storage in soils is due to the additive effect of strong accumulation and stabilisation of OM. We suggest targeting iron oxide-rich soils for soil C sequestration may thus help to bolster climate change mitigation in temperate regions. The finding that land use more substantially affected the mineralisability of illite- than goethite-associted OM also has implications for management, since it suggests that the adoption of sustainable practices to reduce soil OM losses due to environmental change might be especially crucial for soils where mineral assemblages offer little OM stabilisation capability.

Our work also improves the understanding of how mineral composition affects MAOM decomposition in soils. Specifically, we expand the understanding of the role of microorganisms in the differential cycling of phyllosilicate clay- and iron oxide-associated OM in soils by showing that faster decomposition of illite- than goethite-associated OM is likely linked to a higher abundance of microorganisms per unit MAOM on illite than goethite. Our results further suggest that decomposition of MAOM depends not only on the quantity of OM available to mineral-associated microorganisms but also on the presence of available nutrients, with greater constraint of nutrients (in particular of P) on iron oxides than phyllosilicate clays, possibly causing slower cycling of iron oxide- than phyllosilicate clay-associated OM. Deeper investigations of this mineral type–nutrient availability–OM decomposition interaction will be crucial in light of changes in soil nutrient availability that are expected to occur with further intensification of global change drivers, such as elevated CO_2 and N deposition.

Materials and methods

Study sites

The study was conducted on 68 plots, 32 forests and 36 grasslands, across three regions in Germany as part of the *Biodiversity Exploratories*[52] (see Supplementary Table S6 for plot IDs). The study regions are located in southwestern Germany (Schwäbische Alb, ALB), central Germany (Hainich-Dün, HAI), and northeastern Germany (Schorfheide-Chorin, SCH). Soils in ALB and HAI developed on Jurassic limestone and Loess over Triassic limestone, respectively, while those in SCH mainly derive from glacial till covered by glacio-fluvial/aeolian sand. The clay content of the soils ranged from 31.8 to 69.3% in ALB, 16.8–55.2% in HAI, and 0–24.8% in SCH. Soil OC content ranged from 48.1 to 102 g kg^{-1} in ALB, 18.8–85.2 g kg^{-1} in HAI, and 12.8–384 g kg^{-1} in SCH, while soil pH ranged from 3.3 to 7.3 in ALB, 4.1–7.3 in HAI, and 3.4–7.6 in SCH. More details on the pedo-geological characteristics of the study regions are presented in Supplementary Table S5.

Each forest plot covered an area of 100 m × 100 m[52]. Soil OC content in the forest plots ranged from 9.2 to 86.9 g kg^{-1} (mean = 37.1) while soil pH ranged from 3.4 to 6.8 (mean = 4.7 units). Based on the dominant tree species, the plots were categorised as coniferous or deciduous forests. Beech (*Fagus sylvatica* L.) was the dominant deciduous tree species in all study regions. The coniferous forests in ALB and HAI were dominated by spruce (*Picea abies* L.), while those in SCH were dominated by pine (*Pinus sylvestris* L.). We selected nine plots from ALB (three coniferous and six deciduous forests), twelve from HAI (three coniferous and nine deciduous forests), and eleven from SCH (five coniferous and six deciduous forests). The selected ratio of coniferous to deciduous forest plots reflects the typical tree cover and species composition in each region[52]. Of the selected plots, there were six unmanaged (i.e., 3 beech-dominated forests in HAI and 3 in SCH) and 26 managed forests. The basal area of the selected stands ranged from 7.08 to 52.8 m^2 ha^{-1}.

The grassland plots are 50 m × 50 m in size and include meadows that are fertilised and mown; pastures that are fertilised, mown, and grazed; and pastures that are grazed but not mown or fertilised[52]. The intensity of fertilisation, grazing, and mowing (as calculated according to Blüthgen et al.[53], using the calculation tool of Ostrowski et al.[54] implemented in the Biodiversity Exploratories Information System) ranged from 0 to 294 kg N ha^{-1} yr^{-1}, 0–1020 livestock units days ha^{-1} yr^{-1} and 0–3 cuts yr^{-1}. We selected nine plots from ALB and HAI and eighteen from SCH. Nine of the grasslands in SCH were on organic soils (degraded Histosols). At these sites, we exposed the mineral containers to the histic surface horizon. The soil OC content and pH differed between the two grassland types, with both parameters being lower for those on minerals soils (mean soil OC content and pH = 47.4 g kg^{-1} and 6.4 units; range = 21.5–102 g kg^{-1} and 4.7–7.4 units) than on organic soils (mean soil OC content and pH = 152 g kg^{-1} and 7.2 units; range = 76.5–384 g kg^{-1} and 5.5–7.6). We distinguish between grasslands on organic soils and grasslands on mineral soils in our statistical analyses, given the difference in soil physicochemical properties and likely differences in their biological and hydrogeological properties. Since MAOM mineralisability and extractability did not differ between coniferous and deciduous forests, we do not distinguish between forest types.

Experimental design

A detailed description of the experimental design can be found in Bramble et al.[12]. Briefly, five replicates of mineral containers per mineral type were buried in 1 m × 1 m subplots at 5 cm soil depth between November 2015

and January 2016. Each mineral container had a surface area of 35 cm^2 and consisted of a plastic ring bound by a 50-µm mesh on its upper and lower side (Supplementary Fig. S1; Brandt et al.[23]). The mesh prevented the ingrowth of roots and mineral losses, as well as the transport of large particulate OM into the containers, but allowed for water passage and microbial colonisation. Given the container design, translocation of OM into the containers can result from (i) transport of DOM from soil OM decomposition or root exudates via the soil solution, (ii) transport of small (<50 µm) particulate material and microbes by percolating soil water, and (iii) ingrowth of fungi followed by transport of OM and bacteria via fungal hyphae (see Frey et al.[55] and See et al.[56]). The containers were filled with either a mixture of 12 g of synthetic goethite (Bayferrox® 920 Z, CAS-No. 51274-00-1, Lanxess AG, Cologne, Germany) and 12 g of washed and annealed sea sand (VWR, CAS-No. 14808-60-7; <63 µm) or 12 g of natural illite (Inter-ILI. Engineering Co. Ltd., Kosd, Hungary) and 33 g of sea sand. Sea sand was added to improve the water flow through the containers. We ensured the volume of material was the same in the two types of containers. Therefore, illite was mixed with more sand because it had a higher bulk density than goethite. Selected properties of the minerals are presented in the supplementary material.

Sample collection and preparation

Three of the five mineral containers per mineral type were collected in August 2020 after circa five years of field exposure[12]. Soil overlying the containers was also sampled, and a composite was created for each mineral type. All samples were transported to the laboratory in cooling boxes for further processing. The mineral containers were opened in the laboratory, and, if necessary, ingrown hyphae were removed. We also weighed the contents of the mineral containers to account for potential losses during the five-year field exposure. We did not observe any difference in the dry mass of the minerals in the containers during the experimental period. This suggests that there were no significant losses[12]. Nevertheless, as we aimed at determining elemental concentrations, potential MAOM mineralisation, and microbial properties but not stocks or fluxes, potential small losses of minerals are not relevant to the objectives of our study. The three replicates per mineral type were combined and homogenised. An aliquot of the homogenised sample was freeze-dried and ground for elemental analysis, while the remaining sample was stored at −20 °C for microbial analyses and extraction experiments. The moisture content of the fresh mineral sample was calculated as the difference in weight before and after freeze-drying. Soil samples were initially sieved to <4 mm, and then finally to <2 mm prior to storage and analysis. A portion was air-dried and ground while the remaining sample was stored at −20 °C. An aliquot of the air-dried sample was ball-milled for elemental analysis. The moisture content of the soil samples was determined by drying 2-g aliquots at 105 °C for 24 h.

Elemental analyses

Total C (TC) and total nitrogen (TN) concentration of the field-exposed mineral and overlying soil samples were determined by dry combustion at 1100 °C using a varioMAX Cube elemental analyser (Analysensysteme GmbH, Langenselbold, Germany). We determined the soil samples' inorganic C (IC) concentration after combustion at 450 °C to remove OC with the same analyser[12]. The OC concentration of these samples was calculated as the difference between TC and IC. The IC concentration of the mineral samples was determined on a soliTIC module interfaced with the varioMAX Cube elemental analyser[12]. Since the IC concentration on the minerals was negligible, TC equates to OC. We refer to the OC accumulating in the exposed containers as mineral-associated but do not imply that all of the OC therein is chemically bound (i.e., by sorption) to the surfaces of the contained reactive minerals. Noteworthy, however, MAOM does not only include OM that is chemically bound by mineral surfaces but also that which is occluded within micropores or small aggregates formed by the interaction of mineral particles[4]. This also includes particle OM < 53–63 µm. The mesh size of 50 µm ensured that the size of all organic matter in the mineral containers was in the size domain of microaggregates[4,57] and smaller than the upper size limit by which MAOM defined[4] (i.e., 53 µm). Given the twofold difference in specific surface area (SSA) of goethite (20.4 $m^2\ g^{-1}$) and illite (40.7 $m^2\ g^{-1}$), we expressed the amount of accumulated OC per m^2 of pristine mineral (OC concentrations expressed per gram of dry sample are presented in Supplementary Table S1). Note, although the mineral containers contained different ratios of sand to pristine minerals, the very small specific surface area (SSA) and negligible OM sorption capacity of quartz imply that sorption of OC in the containers can be solely ascribed to the contained reactive minerals[12].

The NO_3–N and NH_4–N concentration in 1 M KCl extracts (1:5 sample: extract ratio) was measured photometrically using a SANSplus flow injection analyser (Skalar Analytical B.V., Breda, The Netherlands) to quantify the concentration of exchangeable inorganic N (IN) on the mineral samples. The concentration of IN in these extracts was negligible. Nevertheless, illite likely contained IN in its interlayers, which is not extractable by KCl[58,59]. The total concentration of P on the minerals was determined by sequential wavelength-dispersive X-ray fluorescence spectroscopy (S8 Tiger Series 2, Bruker AXS, Karlsruhe, Germany) using fused beads prepared with 1 g sample aliquots ashed at 1000 °C; analyses were corrected for loss of ignition (including losses of OC) during ashing.

Organic matter extractability and mineralisability

Organic C on the minerals was extracted with $CaCl_2$ in a 1:5 ratio as an indicator of 'easily extractable', bioavailable, OC. We chose $CaCl_2$ as the extractant since it is commonly used to extract dissolved OC in soils[60]. Briefly, 3 g (oven-dried weight basis) of fresh mineral sample, previously stored at −20 °C, was weighed into a 23 mL glass centrifuge tube (Gebr. Rettberg GmbH®). Fifteen mL of 0.01 M $CaCl_2$ (pH 5.95) was then added to the centrifuge tube which was tightly sealed with a lid and agitated for 16 h on an end-over shaker. After shaking, the sample was centrifuged for 30 min at 3500 × *g*. The supernatant was passed through a glass fiber filter with a pore size of 0.6 µm (MACHEREY-NAGEL®) and then stored overnight in 20 mL glass vials (Wheaton®) at 4 °C until analysis. At the time of analysis, 0.7 mL of 10% HCl was added to a 10-mL aliquot of the sample to remove any IC therein. The concentration of OC in the sample was then measured with a varioTOC analyser (Elementar Analysensysteme GmbH). We expressed the concentration of $CaCl_2$ extractable OC as a proportion of the OC concentration on the minerals as an indicator of the extractability of MAOM-C.

The field-exposed mineral samples were incubated under laboratory conditions (20 °C) to determine potential OC mineralisation. For each plot, two grams of fresh mineral sample, previously stored at −20 °C, was weighed into a 20 mL glass vial (ROTILABO ®). Deionised water was added to bring the sample to 60% water holding capacity (WHC; 0.39 and 0.19 $g\ g^{-1}$ for goethite and illite samples, respectively). The vials were then closed with an ND20 butyl stopper (ROTILABO ®) and sealed with a crimp cap. The vials were flushed with CO_2-free air to expel ambient CO_2. They were then pre-incubated in the dark for three days (time determined in preliminary experiments) at 20 °C to allow the microbial community to acclimate to their new conditions and to minimise the anticipated stimulated microbial decomposition of OM caused by the thawing of the previously frozen samples. For quality control, vials flushed with CO_2 free air ($n = 3$) or standard gas (3415 ppm CO_2; $n = 3$) were also incubated with the samples. Since we handled all samples in the same manner and were more interested in comparisons between the mineral and land use treatments than the absolute values of CO_2 release, potential artifacts in CO_2 release, arising from incubating previously frozen samples, are not relevant to the objectives of our study. We quantified the concentration of CO_2 released during the 3-day pre-incubation period by placing the vials on the autosampler (HS-20 series) of a Shimadzu Nexis Gas Chromatograph (GC)−2030. Assuming the density of CO_2 at 20 °C of 1.839 $g\ L^{-1}$, the measured concentrations of CO_2 were converted from units of volume to units of mass. Carbon dioxide release was then expressed as µg C g dry $sample^{-1}$. At the end of this analysis, vials were opened to replenish oxygen and water, if necessary. They were again sealed and incubated firstly for 3, then for 4 and 7 days for a total of

14 days post pre-incubation. Since we were interested in assessing the stability of MAOM, our incubation was kept relatively short to minimise the recycling of microbial products. We calculated the cumulative amount of CO_2 released over the 14-day post-incubation period by summing the concentration of CO_2 measured at the three sampling times. The patterns in CO_2 released during the 3-day pre-incubation mirrored those observed for the 14 days post-incubation (Supplementary Fig. S1). Therefore, we only consider the 14-day post-incubation period in our calculation of MAOM mineralisability (i.e., CO_2 release normalised by the concentration of OC in the mineral containers). We repeated incubations for randomly selected samples ($n = 5$) to assess the precision of our incubation procedure. The coefficient of variation for these samples ranged from 1.31 to 4.17%, validating the repeatability of the procedure.

Phospholipid fatty acids and potential extracellular enzyme activities

We categorised major microbial groups by phospholipid fatty acids (PLFAs) analysis. Briefly, 12 g of sample, previously stored at −20 °C, was thawed and phospholipids were extracted using a single-phase mixture of chloroform, methanol, and aqueous citrate buffer (Bligh and Dyer reagent). Extracted phospholipids were then isolated by phase separation[61]. A mild alkaline methanolysis was used to transform the separated phospholipids into fatty acid methyl esters (FAMEs). Extracted FAMEs were then measured by gas chromatography[23]. The PLFAs i15:0, a 15:0, i16:0, and i17:0 were used as indicators of gram-positive bacteria. Gram-negative bacteria were estimated by PLFAs cy17:0 and cy19:0, and fungi by 18:2ω6,9[62]. Total bacterial PLFAs were calculated as the sum of PLFAs derived from gram-positive and gram-negative bacteria and the fatty acid 16:1ω7. Total PLFA content, calculated as the sum of bacterial and fungal PLFAs, was used as an indicator of microbial biomass. The PLFAs of individual microbial groups were used to calculate the fungi:bacteria ratio and gram-positive: gram-negative bacteria ratio. We estimated the metabolic quotient (qCO_2) of the microbial communities colonising the minerals by normalising the cumulative amount of CO_2 released over the 14-day incubation to the total PLFA content. We are aware that freeze-thawing can lead to the lysis of microbial cells and that this may impact the absolute and relative content of PLFA (microbial biomass) in our samples. Nevertheless, comparisons between treatments are valid since all samples were handled in the same manner.

Potential activities of C-, N-, and P-cycling enzymes—β-glucosidase (BG) (EC 3.2.1.21), β-xylosidase (XYL) (EC 3.2.1.370), N-acetyl-β-glucosaminidase (NAG) (EC 3.2.1.52), and acid phosphatase (AP) (EC 3.1.3.2)—were analysed using fluorogenic substrates[63]. The substrates, containing the fluorescent compound 4-methlumbeliferone (4-MUF), were obtained from Sigma-Aldrich (USA). Enzyme activities were measured spectroscopically on a fluorescence microplate reader (FLX 800, microplate Fluorescence reader, Bio-Tek Instruments Inc., USA) after 0, 30, 60, 120,180, 240, and 300 min (see Brandt et al.[23] for additional details on these measurements). While individual enzymes can reveal differences in the absolute levels of activity between samples, they provide little information about the overall behaviour and nutritional status of the microbial community[39,64]. Thus, we performed vector analysis on the untransformed enzyme activities to infer the relative resource allocation of mineral-associated microorganisms toward C, N, and P acquisition[39]. Vector lengths inform on the relative investment in C vs. nutrient (N and P) acquisition. They are calculated using equation (1), where x represents the relative activities of C- vs. P-acquiring enzymes ($(BG + XYL/BG + XYL + AP)$) and y represents the relative activities of C- vs. N-acquiring enzymes ($(BG + XYL)/BG + XYL + NAG$). Lower vector lengths indicate an increase in microbial investment in nutrients relative to C acquisition and, potentially, an increase in nutrient limitation[39].

$$Vector\ length = \sqrt{(x^2 + y^2)} \quad (1)$$

Vector angles inform on the relative investment in N vs. P acquisition and were calculated as the arctangent of the line extending from the plot origin point (x, y) according to Eq. 2.

$$\text{Vector angle}\,(^\circ) = \text{degrees}\,(\text{atan2}(x, y)) \quad (2)$$

Higher vector angles indicate an increase in microbial investment in P relative to N acquisition and, potentially, an increase in P limitation[39]. We previously found that vector angles were negatively correlated with sodium bicarbonate-extractable organic P (i.e., an indicator of bioavailable organic P) across different sites for both goethite and illite[24]. This indicates increasing investment in P relative to N acquisition when organic P content decreased, demonstrating the usefulness of vector angles as an indicator of microbial P limitation.

Statistical analyses

All statistical analyses were carried out in R (version 4.3.2, R core Team, 2023). Analysis of variance (ANOVA) was carried out using the *aov* function to assess the main and interactive effects of categorical variables of interest (i.e., land use and mineral type) on the various response variables. We accounted for the effect of the study region by including it as the first factor in the ANOVA. Histograms and Q-Q plots were used to check that the data were normally distributed. We used scatter plots of standardised residuals against fitted values to verify that the assumption of homogenous variance was not violated. If necessary, response variables were log-transformed to meet model assumptions. Tukey's honest significant difference test was used to assess differences between means. Cohen's F (partial) effect size of the factors in the ANOVA was calculated using the cohens_f function from the package effect size[65]. Variances from the ANOVA were partitioned using the calc. relimp function (type = "lmg") from the relaimpo package[66]. All plots were created using ggplot2[67].

To gain insight into mechanisms behind the effect of mineral type and land use on MAOM mineralisability, we ran linear mixed-effect models — one for mineral type and one for land use— with the function lmer from the R package lme4[68]. The PLFA:MAOM-C ratio, MAOM extractability and enzymatic vector angles (as an indicator of P availability) were chosen as factors that likely underlie the 'mineral type effect'. The decision to only include these variables in the 'mineral type' effect model was based on prior hypotheses and the results from the ANOVAs in our study. Land use and study region were considered as random factors in the model. Using the same selection criteria, we included the enzymatic vector length (as an indicator of nutrient limitation), fungi:bacteria ratio, GP:GN bacteria ratio, PLFA-normalised BG and PLFA-normalised XYL activity as fixed factors that likely underlie the land use effect. Although the ANOVAs showed a significant effect of land use on qCO_2, this variable was not included in the 'land use' effect model because, like MAOM mineralisability, it is calculated using CO_2 release. Mineral type and study region were considered a random factor in the 'land use effect' model. The same quality assurance measures used for the ANOVAs were carried out to verify that the assumptions of the linear mixed effect models were met. Variance inflation factors were calculated using the vif function from the car package[69] to assess multicollinearity. The VIFs were <3, indicating no multicollinearity issue in our models[70]. The Anova and rmse functions of the car package were used to extract P-values and root mean square error (RMSE) values, respectively, for the models. R^2 values were extracted with the function r.squaredGLMM from the MuMIn package[71]. Variances from the models were partitioned using the r2beta function (method = 'nsj') from package r2glmm[72].

Reporting summary

Further information on research design is available in the Nature Portfolio Reporting Summary linked to this article.

Data availability

This work is based on data collected within the BEmins project and Core Project 9 of the Biodiversity Exploratories (DFG Priority Program 1374). The datasets generated during this project are deposited in the Biodiversity Exploratories Information System, BExIS (https://www.bexis.uni-jena.de/).

The datasets can be accessed using the following IDs: 14686 (soil texture[73]), 17026 (mineral soil respiration[74]), 22246 (soil pH[75]), 31251 (mineral-associated organic C and total N contents, and soil C and N contents[12,76]), 31316 (enzyme activities[23,24,77]), 31317 (PLFAs[23,24,78]), 31772 (MAOM mineralisation and mineralisability[79]), 31773 (MAOM extractability[80]), and 31774 (mineral-associated total P content[81]). Supplementary Tables S5 and S6 were uploaded to Figshare (https://doi.org/10.6084/m9.figshare.29087513).

Code availability

No custom code was used to generate or process the data described in the manuscript. All steps involved in data processing have been duly described in the Materials and Methods section.

Received: 15 July 2024; Accepted: 19 May 2025;
Published online: 27 May 2025

References

1. Georgiou, K. et al. Global stocks and capacity of mineral-associated soil organic carbon. *Nat. Commun.* **13**, 3797 (2022).
2. Sokol, N. W. et al. Global distribution, formation and fate of mineral-associated soil organic matter under a changing climate: a trait-based perspective. *Funct. Ecol.* **36**, 1411–1429 (2022).
3. Sokol, N. W., Sanderman, J. & Bradford, M. A. Pathways of mineral-associated soil organic matter formation: integrating the role of plant carbon source, chemistry, and point of entry. *Glob. Change Biol.* **25**, 12–24 (2019).
4. Lavallee, J. M., Soong, J. L. & Cotrufo, M. F. Conceptualizing soil organic matter into particulate and mineral-associated forms to address global change in the 21st century. *Glob. Change Biol.* **26**, 261–273 (2020).
5. Mikutta, R. et al. Biodegradation of forest floor organic matter bound to minerals via different binding mechanisms. *Geochim. et. Cosmochim. Acta* **71**, 2569–2590 (2007).
6. Eusterhues, K., Neidhardt, J., Hädrich, A., Küsel, K. & Totsche, K. U. Biodegradation of ferrihydrite-associated organic matter. *Biogeochemistry* **119**, 45–50 (2014).
7. Hemingway, J. D. et al. Mineral protection regulates long-term global preservation of natural organic carbon. *Nature* **570**, 228–231 (2019).
8. Kleber, M. et al. Mineral–organic associations: formation, properties, and relevance in soil environments. *Adv. Agron.* **130**, 1–140 (2015).
9. Jones, D. & Edwards, A. Influence of sorption on the biological utilization of two simple carbon substrates. *Soil Biol. Biochem.* **30**, 1895–1902 (1998).
10. Konrad, A. et al. Microbial carbon use efficiency of mineral-associated organic matter is related to its desorbability. *Soil Biol. Biochem.* **203**, 109740 (2025).
11. Torn, M. S., Trumbore, S. E., Chadwick, O. A., Vitousek, P. M. & Hendricks, D. M. Mineral control of soil organic carbon storage and turnover. *Nature* **389**, 170–173 (1997).
12. Bramble, D. S. E. et al. Formation of mineral-associated organic matter in temperate soils is primarily controlled by mineral type and modified by land use and management intensity. *Glob. Change Biol.* **30**, e17024 (2024).
13. Schrumpf, M. et al. Storage and stability of organic carbon in soils as related to depth, occlusion within aggregates, and attachment to minerals. *Biogeosciences* **10**, 1675–1691 (2013).
14. Rasmussen, C. et al. Beyond clay: towards an improved set of variables for predicting soil organic matter content. *Biogeochemistry* **137**, 297–306 (2018).
15. von Fromm, S. F. et al. Controls on timescales of soil organic carbon persistence across sub-Saharan Africa. *Glob. Change Biol.* **30**, e17089 (2024).
16. Kirsten, M. et al. Iron oxides and aluminous clays selectively control soil carbon storage and stability in the humid tropics. *Sci. Rep.* **11**, 5076 (2021).
17. Guhra, T., Ritschel, T. & Totsche, K. U. Formation of mineral–mineral and organo–mineral composite building units from microaggregate-forming materials including microbially produced extracellular polymeric substances. *Eur. J. Soil Sci.* **70**, 604–615 (2019).
18. Guhra, T., Stolze, K. & Totsche, K. U. Pathways of biogenically excreted organic matter into soil aggregates. *Soil Biol. Biochem.* **164**, 108483 (2022).
19. Saidy, A., Smernik, R., Baldock, J. A., Kaiser, K. & Sanderman, J. The sorption of organic carbon onto differing clay minerals in the presence and absence of hydrous iron oxide. *Geoderma* **209**, 15–21 (2013).
20. Saidy, A. R., Smernik, R., Baldock, J., Kaiser, K. & Sanderman, J. Microbial degradation of organic carbon sorbed to phyllosilicate clays with and without hydrous iron oxide coating. *Eur. J. Soil Sci.* **66**, 83–94 (2015).
21. Liang, G., Stark, J. & Waring, B. G. Mineral reactivity determines root effects on soil organic carbon. *Nat. Commun.* **14**, 4962 (2023).
22. Cao, Y. et al. Preferential adsorption of extracellular polymeric substances from bacteria on clay minerals and iron oxide. *Colloids Surf. B: Biointerfaces* **83**, 122–127 (2011).
23. Brandt, L. et al. Mineral type and land-use intensity control composition and functions of microorganisms colonizing pristine minerals in grassland soils. *Soil Biol. Biochem.* **182**, 109037 (2023).
24. Brandt, L. et al. Mineral type versus environmental filters: What shapes the composition and functions of fungal communities in the mineralosphere of forest soils?. *Soil Biol. Biochem.* **190**, 109288 (2024).
25. Labouyrie, M. et al. Patterns in soil microbial diversity across Europe. *Nat. Commun.* **14**, 3311 (2023).
26. Kaiser, K. et al. Driving forces of soil bacterial community structure, diversity, and function in temperate grasslands and forests. *Sci. Rep.* **6**, 33696 (2016).
27. Solly, E. F. et al. Factors controlling decomposition rates of fine root litter in temperate forests and grasslands. *Plant Soil* **382**, 203–218 (2014).
28. Zhang, J. et al. C : N : P stoichiometry interrestrial ecosystems in China. *Sci. Total Environ.* **795**, e148849 (2021).
29. Dong, L. et al. Forests have a higher soil C sequestration benefit due to lower C mineralization efficiency: evidence from the central loess plateau case. *Agric. Ecosyst. Environ.* **339**, 108144 (2022).
30. Gan, H. Y. The effects of land use and management on belowground carbon and nutrient interactions. PhD thesis, Friedrich-Schiller-Universität, Jena (2019).
31. Fanin, N. et al. The ratio of Gram-positive to Gram-negative bacterial PLFA markers as an indicator of carbon availability in organic soils. *Soil Biol. Biochem.* **128**, 111–114 (2019).
32. Elias, D. M. et al. Microbial and mineral interactions decouple litter quality from soil organic matter formation. *Nat. Commun.* **15**, 10063 (2024).
33. Roller, B. R. & Schmidt, T. M. The physiology and ecological implications of efficient growth. *ISME J.* **9**, 1481–1487 (2015).
34. Malik, A. A. et al. Land use driven change in soil pH affects microbial carbon cycling processes. *Nat. Commun.* **9**, 3591 (2018).
35. Herold, N., Schöning, I., Michalzik, B., Trumbore, S. & Schrumpf, M. Controls on soil carbon storage and turnover in German landscapes. *Biogeochemistry* **119**, 435–451 (2014).
36. Heckman, K. A. et al. Divergent controls on carbon concentration and persistence between forests and grasslands of the conterminous US. *Biogeochemistry* **156**, 41–56 (2021).
37. Chen, C., Hall, S. J., Coward, E. & Thompson, A. Iron-mediated organic matter decomposition in humid soils can counteract protection. *Nat. Commun.* **11**, 1–13 (2020).
38. Cui, Y. et al. Ecoenzymatic stoichiometry reveals widespread soil phosphorus limitation to microbial metabolism across Chinese forests. *Commun. Earth Environ.* **3**, 184 (2022).

39. Moorhead, D. L., Sinsabaugh, R. L., Hill, B. H. & Weintraub, M. N. Vector analysis of ecoenzyme activities reveal constraints on coupled C, N and P dynamics. *Soil Biol. Biochem.* **93**, 1–7 (2016).
40. Abay, P., Gong, L., Luo, Y., Zhu, H. & Ding, Z. Soil extracellular enzyme stoichiometry reveals the nutrient limitations in soil microbial metabolism under different carbon input manipulations. *Sci. Total Environ.* **913**, 169793 (2024).
41. He, P., Zhang, Y., Shen, Q., Ling, N. & Nan, Z. Microbial carbon use efficiency in different ecosystems: a meta-analysis based on a biogeochemical equilibrium model. *Glob. Change Biol.* **29**, 4758–4774 (2023).
42. Sinsabaugh, R. L. & Follstad Shah, J. J. Ecoenzymatic stoichiometry and ecological theory. *Annu. Rev. Ecol. Evol. Syst.* **43**, 313–343 (2012).
43. Wu, S., Konhauser, K. O., Chen, B. & Huang, L. "Reactive Mineral Sink" drives soil organic matter dynamics and stabilization. *npj Mater. Sustain.***1**, 3 (2023).
44. Stoner, S. et al. Relating mineral–organic matter stabilization mechanisms to carbon quality and age distributions using ramped thermal analysis. *Philos. Trans. R. Soc. A* **381**, 20230139 (2023).
45. Jilling, A. et al. Minerals in the rhizosphere: overlooked mediators of soil nitrogen availability to plants and microbes. *Biogeochemistry* **139**, 103–122 (2018).
46. Heckman, K. A. et al. Moisture-driven divergence in mineral-associated soil carbon persistence. *Proc. Natl. Acad. Sci. USA* **120**, e2210044120 (2023).
47. Cao, T., Luo, Y., Shi, M., Tian, X. & Kuzyakov, Y. Microbial interactions for nutrient acquisition in soil: miners, scavengers, and carriers. *Soil Biol. Biochem.* **188**, 109215 (2023).
48. Kallenbach, C. M., Frey, S. D. & Grandy, A. S. Direct evidence for microbial-derived soil organic matter formation and its ecophysiological controls. *Nat. Commun.* **7**, 13630 (2016).
49. Feng, J. et al. Soil microbial trait-based strategies drive metabolic efficiency along an altitude gradient. *ISME Commun.* **1**, 71 (2021).
50. Eusterhues, K. et al. Importance of inner-sphere PO-Fe bonds in natural and synthetic mineral-organic associations. *Sci. Total Environ.* **905**, 167232 (2023).
51. Spohn, M. Preferential adsorption of nitrogen-and phosphorus-containing organic compounds to minerals in soils: a review. *Soil Biol. Biochem.* **194**, 109428 (2024).
52. Fischer, M. et al. Implementing large-scale and long-term functional biodiversity research: the biodiversity exploratories. *Basic Appl. Ecol.* **11**, 473–485 (2010).
53. Blüthgen, N. et al. A quantitative index of land-use intensity in grasslands: integrating mowing, grazing and fertilization. *Basic Appl. Ecol.* **13**, 207–220 (2012).
54. Ostrowski, A., Lorenzen, K., Petzold, E. & Schindler, S. Land use intensity index (LUI) calculation tool of the Biodiversity Exploratories project for grassland survey data from three different regions in Germany since 2006, BEXIS 2 module. *Zenodo* https://doi.org/10.5281/zenodo.3865579 (2020).
55. Frey, S. D., Six, J. & Elliott, E. Reciprocal transfer of carbon and nitrogen by decomposer fungi at the soil–litter interface. *Soil Biol. Biochem.* **35**, 1001–1004 (2003).
56. See, C. R. et al. Hyphae move matter and microbes to mineral microsites: Integrating the hyphosphere into conceptual models of soil organic matter stabilization. *Glob. Change Biol.* **28**, 2527–2540 (2022).
57. Totsche, K. U. et al. Microaggregates in soils. *J. Plant Nutr. Soil Sci.* **181**, 104–136 (2018).
58. Gouveia, G. & Eudoxie, G. Relationship between ammonium fixation and some soil properties and effect of cation treatment on fixed ammonium release in a range of Trinidad soils. *Commun. Soil Sci. Plant Anal.* **33**, 1751–1765 (2002).
59. Nieder, R., Benbi, D. K. & Scherer, H. W. Fixation and defixation of ammonium in soils: a review. *Biol. Fertil. Soils* **47**, 1–14 (2011).
60. Houba, V., Temminghoff, E., Gaikhorst, G. & Van Vark, W. Soil analysis procedures using 0.01 M calcium chloride as extraction reagent. *Commun. Soil Sci. Plant Anal.* **31**, 1299–1396 (2000).
61. Frostegård, Å, Tunlid, A. & Bååth, E. Microbial biomass measured as total lipid phosphate in soils of different organic content. *J. Microbiol. Methods* **14**, 151–163 (1991).
62. Ruess, L. & Chamberlain, P. M. The fat that matters: soil food web analysis using fatty acids and their carbon stable isotope signature. *Soil Biol. Biochem.* **42**, 1898–1910 (2010).
63. Marx, M.-C., Wood, M. & Jarvis, S. A microplate fluorimetric assay for the study of enzyme diversity in soils. *Soil Biol. Biochem.* **33**, 1633–1640 (2001).
64. Moorhead, D. L., Rinkes, Z. L., Sinsabaugh, R. L. & Weintraub, M. N. Dynamic relationships between microbial biomass, respiration, inorganic nutrients and enzyme activities: informing enzyme-based decomposition models. *Front. Microbiol.* **4**, 56126 (2013).
65. Ben-Shachar, M. S., Lüdecke, D. & Makowski, D. effectsize: Estimation of effect size indices and standardized parameters. *J. Open Source Softw.* **5**, 2815 (2020).
66. Grömping, U. Relative importance for linear regression in R: the package relaimpo. *J. Stat. Softw.* **17**, 1–27 (2007).
67. Wickham, H. & Wickham, H. *ggplot2: Elegant Graphics for Data Analysis* Springer (2016).
68. Bates, D., Mächler, M., Bolker, B. & Walker, S. Fitting linear mixed-effects models using lme4. *J. Stat. Softw.* **67**, 1–48 (2015).
69. Fox, J. & Weisberg, S. *An R companion to applied regression*. (Sage Publications, 2018).
70. Zuur, A. F., Ieno, E. N. & Elphick, C. S. A protocol for data exploration to avoid common statistical problems. *Methods Ecol. Evol.***1**, 3–14 (2010).
71. Barton, K. MuMIn: multi-model inference. http://r-forger-project.org/projects/mumin/, (2009).
72. Jaeger, B. C., Edwards, L. J., Das, K., Sen, P. K. & An, R. 2 statistic for fixed effects in the generalized linear mixed model. *J. Appl. Stat.* **44**, 1086–1105 (2017).
73. Schöning, I., Solly, E., Klötzing, T., Trumbore, S. & Schrumpf, M. MinSoil 2011 - Soil Texture. v10. *Biodiversity Exploratories Information System*. *Dataset*. https://www.bexis.uni-jena.de/ddm/data/Showdata/14686?version=10 (2021).
74. Schöning, I., Solly, E., Klötzing, T., Trumbore, S. & Schrumpf M. Soil sampling campaign 2011, all experimental plots (EP), 0-10 cm - mineral soil respiration. v5. *Biodiversity Exploratories Information System. Dataset*. https://www.bexis.uni-jena.de/ddm/data/Showdata/17026?version=5 (2023).
75. Schöning, I., Klötzing, T., Trumbore, S. & Schrumpf, M. Soil pH - soil sampling campaign 2017, all experimental plots (EPs), 0-10 cm. v6. *Biodiversity Exploratories Information System. Dataset*. https://www.bexis.unijena.de/ddm/data/Showdata/22246?version=6 (2024).
76. Bramble, D. S., Ulrich, S., Schöning, I., Kaiser, K. & Schrumpf, M. Carbon and nitrogen concentrations in soil and mineral containers at 5 cm depth for all forest and grassland EPs, 2020 (BEmins project). v22. *Biodiversity Exploratories Information System. Dataset*. https://www.bexis.uni-jena.de/ddm/data/Showdata/31251?version=22 (2025).
77. Brandt, L. et al. Enzyme activities in soil and mineral containers, 2020. v16. *Biodiversity Exploratories Information System. Dataset*. https://www.bexis.uni-jena.de/ddm/data/Showdata/31316?version=16 (2024).
78. Brandt, L., Stache, F., Poll, C. & Kandeler, E. Phospholipid fatty acids (PLFAs) in soil and mineral containers (5 cm), 2020. v9. *Biodiversity Explor. Inform. Syst. Dataset*. https://www.bexis.uni-jena.de/ddm/data/Showdata/31317?version=9 (2024).
79. Bramble, D. S., Schöning, I. & Schrumpf, M. Mineral-associated organic carbon mineralization for 68 experimental plots, 2020. v5.

Biodivers. Explor. Inform. Syst. Dataset. https://www.bexis.uni-jena.de/ddm/data/Showdata/31772?version=5 (2025).
80. Bramble, D. S., Schöning, I. & Schrumpf, M. Mineral-associated organic carbon desorbability for 68 experimental plots, 2020.v5. *Biodivers. Explor. Inform. Syst. Dataset*. https://www.bexis.uni-jena.de/ddm/data/Showdata/31773?version=5 (2025).
81. Ulrich, S., Mikutta, R. & Kaiser, K. Mineral-associated total phosphorus for 68 experimental, 2020.v5. *Biodivers. Explor. Inform. System. Dataset*. https://www.bexis.uni-jena.de/ddm/data/Showdata/31774?version=5 (2025).

Acknowledgements

We thank the managers of the three Exploratories, Kirsten Reichel-Jung, Iris Steitz, Sandra Weithmann, Florian Staub, Julia Bass, Juliane Vogt, Anna K. Franke, Miriam Teuscher, Franca Marian, and all former managers for their work in maintaining the plot and project infrastructure; Christiane Fischer, Jule Mangels, and Victoria Grießmaier for support through the central office, Michale Owonibi and Andreas Ostrowski for managing the central database, and Markus Fischer, Eduard Linsenmair, Dominik Hessenmöller, Daniel Prati, François Buscot, Ernst-Detlef Schulze, Wolfgang W. Weisser, and the late Elisabeth Kalko for their role in setting up the Biodiversity Exploratories project. We thank the administration of the Hainich national park, the UNESCO Biosphere Reserve Schwäbische Alb, and the UNESCO Biosphere Reserve Schorfheide-Chorin as well as all land owners for the excellent collaboration. We further thank Ines Hilke, Birgit Froehlich, Jessica Heublein, and Petra Linke of the Routine Measurements & Analysis of Environmental Samples (ROMA) laboratory at the Max Planck Institute for Biogeochemistry (MPI-BGC), Fabian Stache, Moritz Mainka, Alexandra Boritzki, Christine Krenkewitz, Gudrun Nemson-von Koch, Anja Kroner, Miriam Kempe, Steffen Ferber, Marco Pöhlmann, Theresa Klötzing, Iris Kuhlmann, Sarah Pozorski, Uzma Heme, Stephanie Strahl, Manuel Rost, Enrico Weber, Adrian Lattacher, Philipp Mäder, Juliette Blum, and Marina Patulla for support during sampling and laboratory analyses. We thank Susan Trumbore and Gerd Gleixner for their comments that helped to improve the manuscript, Thomas Wultzer for creating an R script to extract the Gas Chromatography data, and Armin Jordan and Johannes Schwarz of the ICOS-FCL service group, MPI-BGC, for preparing the standards used to calibrate the Gas Chromatograph analyser. Fieldwork permits were issued by the responsible state environmental offices of Baden-Württemberg, Thüringen, and Brandenburg. This work was funded by the DFG Priority Program 1374 “Biodiversity-Exploratories” (DFG project numbers 433273584 and 193957772) and the Max Planck Society. Funding for De Shorn E. Bramble was provided by the International Max Planck Research School for Biogeochemical Cycles (IMPRS-gBGC).

Author contributions

D.E.B.: conceived the study, wrote the manuscript, conducted the incubation experiments, performed laboratory analyses, collected and analysed data, performed the statistical analyses, and created the figures. I.S.: established the original field experiment, conceived the study, supervised D.E.B. and revised the manuscript. L.B.: performed laboratory analyses, collected and analysed data, and created Fig. 4. C.P.: supervised L.B. and revised the manuscript; E.K. conceived the study, acquired funding, supervised L.B., and revised the manuscript. S.U.: performed laboratory analyses, and collected and analysed data. R.M.: conceived the study, acquired funding, supervised S.U., and revised the manuscript. C.M.: conceived the study, acquired funding, and revised the manuscript. W.L.S.: supervised D.E.B. and revised the manuscript. K.U.T.: supervised D.E.B. and revised the manuscript. K.K.: conceived the study, acquired funding, and revised the manuscript, and supervised S.U. and D.E.B. M.S.: established the original field experiment, conceived the study, acquired funding, supervised D.E.B. and revised the manuscript.

Funding

Open Access funding enabled and organized by Projekt DEAL.

Competing interests

The authors declare no competing interests.

Additional information

Supplementary information The online version contains supplementary material available at https://doi.org/10.1038/s43247-025-02400-3.

Correspondence and requests for materials should be addressed to De Shorn E. Bramble or Marion Schrumpf.

Peer review information *Communications Earth & Environment* thanks the anonymous reviewers for their contribution to the peer review of this work. Primary Handling Editors: Somaparna Ghosh.

Reprints and permissions information is available at http://www.nature.com/reprints

Publisher’s note Springer Nature remains neutral with regard to jurisdictional claims in published maps and institutional affiliations.

Open Access This article is licensed under a Creative Commons Attribution 4.0 International License, which permits use, sharing, adaptation, distribution and reproduction in any medium or format, as long as you give appropriate credit to the original author(s) and the source, provide a link to the Creative Commons licence, and indicate if changes were made. The images or other third party material in this article are included in the article’s Creative Commons licence, unless indicated otherwise in a credit line to the material. If material is not included in the article’s Creative Commons licence and your intended use is not permitted by statutory regulation or exceeds the permitted use, you will need to obtain permission directly from the copyright holder. To view a copy of this licence, visit http://creativecommons.org/licenses/by/4.0/.

© The Author(s) 2025